http://dx.doi.org/10.18623/rvd.v23.n3.4267

MACHINE LEARNING MODELS (MLP, RANDOM FOREST, LIGHTGBM) FOR DAILY ET_0 ESTIMATION WITH LIMITED DATA IN HUMID MEDITERRANEAN REGION (JIJEL) ALGERIA

MODELOS DE APRENDIZAGEM AUTOMÁTICA (MLP, RANDOM FOREST, LIGHTGBM) PARA A ESTIMATIVA DIÁRIA DE ET_0 COM DADOS LIMITADOS NA REGIÃO MEDITERRÂNICA HÚMIDA (JIJEL), ARGÉLIA

Article received on: 8/29/2025
Article accepted on: 11/28/2025

Assia Meziani*
*Department of Hydraulic and Civil Engineering, New Technology and Local Development Laboratory, Faculty of Technology, University of El-Oued, El-Oued, Algeria.
Orcid: https://orcid.org/0000-0002-2569-1552
assia-meziani@univ-eloued.dz

The authors declare that there is no conflict of interest

Abstract
Accurate estimation of the reference evapotranspiration (ET_0) is essential for effective irrigation planning and sustainable water resource management, particularly in climatically heterogeneous regions. This study evaluated the performance of three machine learning models— multilayer perceptron (MLP), Random Forest (RF), and Light Gradient Boosting Machine (LightGBM)—for predicting daily FAO-56 Penman–Monteith ET_0 in the humid Mediterranean region of Jijel, northeastern Algeria. Daily meteorological data from ten stations for the period 2000–2024 were used, incorporating six input variables: air temperature, relative humidity, wind speed, sunshine duration, solar radiation, and vapor pressure deficit. The model performance was assessed using multiple statistical metrics across the training, validation, and independent testing datasets. All models achieved high predictive accuracy, with R^2 values exceeding 0.97. RF exhibited the highest training performance (R^2 = 0.997, RMSE ≈ 0.09 mm day^{-1}) but showed signs of mild overfitting on test data. In contrast, MLP demonstrated the best generalization capability (test R^2 = 0.983, RMSE = 0.21 mm day^{-1}, NSE = 0.983), closely followed by LightGBM (test R^2 ≈ 0.980). Trend analysis revealed no significant long-term change in annual ET_0 (p = 0.907). The results confirm the robustness of machine learning approaches, particularly MLP and LightGBM, for reliable ET_0 estimation in humid Mediterranean environments.

Keywords: Reference Evapotranspiration. FAO-56. LightGBM. Multi-Layer Perceptron. Random Forest. Jijel. Algeria.

Resumo
A estimativa precisa da evapotranspiração de referência (ET_0) é essencial para o planejamento eficiente da irrigação e a gestão sustentável dos recursos hídricos, especialmente em regiões climaticamente heterogêneas. Este estudo avaliou três modelos de aprendizado automático —Perceptrão Multicamada (MLP), Random Forest (RF) e LightGBM— para prever a ET_0 diária FAO-56 Penman–Monteith na região mediterrânea húmida de Jijel (nordeste da Argélia). Foram utilizados dados meteorológicos diários de dez estações (2000–2024) com seis variáveis: temperatura do ar, humidade relativa, velocidade do vento, duração da insolação, radiação solar e défice de pressão de vapor. O desempenho foi medido com métricas estatísticas em conjuntos de treino, validação e teste. Todos os modelos alcançaram alta precisão (R^2 > 0,97). O RF obteve o melhor desempenho no treino (R^2 = 0,997; RMSE ≈ 0,09 mm dia^{-1}), mas mostrou leve sobreajuste no teste. O MLP apresentou a melhor generalização (R^2 teste = 0,983; RMSE = 0,21 mm dia^{-1}; NSE = 0,983), seguido de perto pelo LightGBM (R^2 teste ≈ 0,980). A análise de tendências não detectou alterações significativas na ET_0 anual (p = 0,907). Os resultados confirmam a robustez dos enfoques de machine learning, especialmente MLP e LightGBM, para estimar ET_0 de forma fiável em ambientes mediterrâneos húmidos.

Palavras-chave: *Evapotranspiração de Referência. FAO-56. LightGBM. Perceptrão Multicamada. Random Forest. Jijel. Argélia.*

1 INTRODUCTION

Reference evapotranspiration (ET_0) is a fundamental parameter in hydrology and agriculture and plays a pivotal role in water resource management, irrigation scheduling, and crop modeling by quantifying the potential water loss from a standardized hypothetical grass crop (ALLEN et al., 1998; MONTEITH, 1965). Accurate ET_0 estimation is especially vital in regions prone to climatic variability, such as the coastal humid zone of Jijel, Algeria, where fluctuations in precipitation and temperature directly influence water availability and agricultural productivity (BOUREGAA, 2025).

Conventional approaches, including the Penman (1948), Hargreaves–Samani (1985), and FAO-56 Penman–Monteith (ALLEN ET AL., 1998) equations, remain benchmarks for ET_0 calculation but demand comprehensive meteorological datasets that are often unavailable or incomplete in many locations (VALIANTZAS, 2013; SHIRI, 2017; AL HASANI & SHAHID, 2024). Consequently, machine learning (ML) techniques have emerged as powerful alternatives for modeling complex nonlinear relationships with limited inputs (FAN et al., 2018; ACHARKI et al., 2025; ELBELTAGI et al., 2024).

Among these, multilayer perceptron (MLP) neural networks effectively capture the nonlinear interactions between meteorological variables and ET_0, demonstrating robust performance in humid, semi-arid, and arid climates (ACHITE et al., 2022; AYAZ et al., 2021; KARTAL, 2024; MEHDIZADEH, 2018; TIKHAMARINE et al., 2020). Random Forest (RF), an ensemble of decision trees, mitigates overfitting, tolerates missing values, and yields reliable predictions (AGRAWAL et al., 2022; KARIMI et al., 2020; ZHOU et al., 2025). Gradient Boosting Decision Trees (GBDT) sequentially refine predictions by minimizing residuals, frequently surpassing traditional and individual learner models (ZHOU et al., 2020; MALIK et al., 2022; PATEL et al., 2025; SZCZEPANEK, 2022).

Recent studies have highlighted the advantages of ML over empirical methods, with advanced techniques including extreme learning machines, hybrid architectures, and deep learning achieving superior accuracy in data-scarce environments (ABDULLAH et al., 2015; ALY et al., 2024; BOUKHALI et al., 2025; CHEN et al., 2020; FAN et al., 2018; WU et al., 2020; RODRIGUES & BRAGA, 2021; ZHOU et al., 2025; TRONCOSO GARCÍA et al., 2023). Ensemble tree-based models such as RF and GBDT have shown consistent excellence across diverse climates (CHANG et al., 2025; STEFANIDIS et al., 2025; LIANG et al., 2023; MANDAL & CHANDA, 2023). Further enhancements through optimization algorithms, attention mechanisms, and bio-inspired methods (e.g., the Grey Wolf Optimizer) have refined

predictive capabilities (HERAMB et al., 2023; YAO et al., 2025; ZHOU et al., 2025; CHEN et al., 2020). In Algeria, ML-driven ET_0 modeling is gaining prominence for bolstering sustainable water management and agriculture, particularly in regions with data limitations or unique climatic features (BOUREGAA, 2025; LADLANI et al., 2012; VALIANTZAS, 2013; SHIRI, 2017; KARIMI et al., 2020). Nonetheless, comprehensive comparative assessments of ML models for FAO-56 ET_0 estimation in the humid coastal context of Jijel remain limited because previous studies have predominantly targeted semi-arid interior zones or contrasting climates.

This knowledge gap constrains insights into model efficacy amid Jijel's specific climatic variability and potential data constraints. The present study addresses this by evaluating the performance of MLP, RF, and GBDT models in estimating FAO-56 reference evapotranspiration in the Jijel region and year-to-year changes in evapotranspiration. By leveraging the complementary strengths of these approaches, this study sought to establish a robust, data-efficient framework for enhancing irrigation efficiency and fostering sustainable agriculture under varying climatic conditions.

2 MATERIALS AND METHODS

2.1 Study area

Jijel Province is a coastal region in northeastern Algeria that borders the Mediterranean Sea to the north (Figure 1). It spans an area of approximately 2,577 km² and features diverse topography, including narrow coastal plains, rolling hills, and mountainous interiors, dominated by the Tell Atlas Range (KERDOUD, 2017). Unlike Algeria, which is predominantly arid, Jijel has a humid Mediterranean climate, making it one of the country's wettest regions (MERNIZ et al., 2019). Winters are mild and rainy, while summers are hot and humid (BOUTELLIS & BOUCHAIR., 2022). Annual precipitation typically ranges from 900 to 1,200 mm, concentrated mainly between October and April (MERNIZ et al., 2019). The mean annual temperature ranges from approximately 10 to 15°C in winter to 25–30°C in summer.

This combination of abundant rainfall and high humidity imparts a sub-humid to humid character to the region, profoundly influencing its hydrology, dense vegetation cover, and the availability of water resources. Topographic variability, from sea level along the coast to elevations exceeding 1,000 m in the Tell Atlas, further generates localized microclimates, posing significant challenges for water resource management and agricultural planning.

This study used meteorological data from six representative stations distributed across the province: Jijel(36.82° N, 5.77° E), Taher (36.77° N, 5.90° E), Chekfa (36.65° N, 6.00° E), Djimla (36.55° N, 5.53° E), El Ancer (36.80° N, 5.98° E), El Kennar Nouchfi (36.73° N, 5.85° E), El Milia (36.75° N, 6.27° E), Emir Abdelkader (36.80° N, 5.80° E), Kaous (36.65° N, 5.85° E), and Tassoust (36.70° N, 5.95° E) (Figure 1). These sites capture the climatic and topographic heterogeneity of the region.

Figure 1

Localization of 10 studied stations in Jijel region (Algeria) (https://d-maps.com).

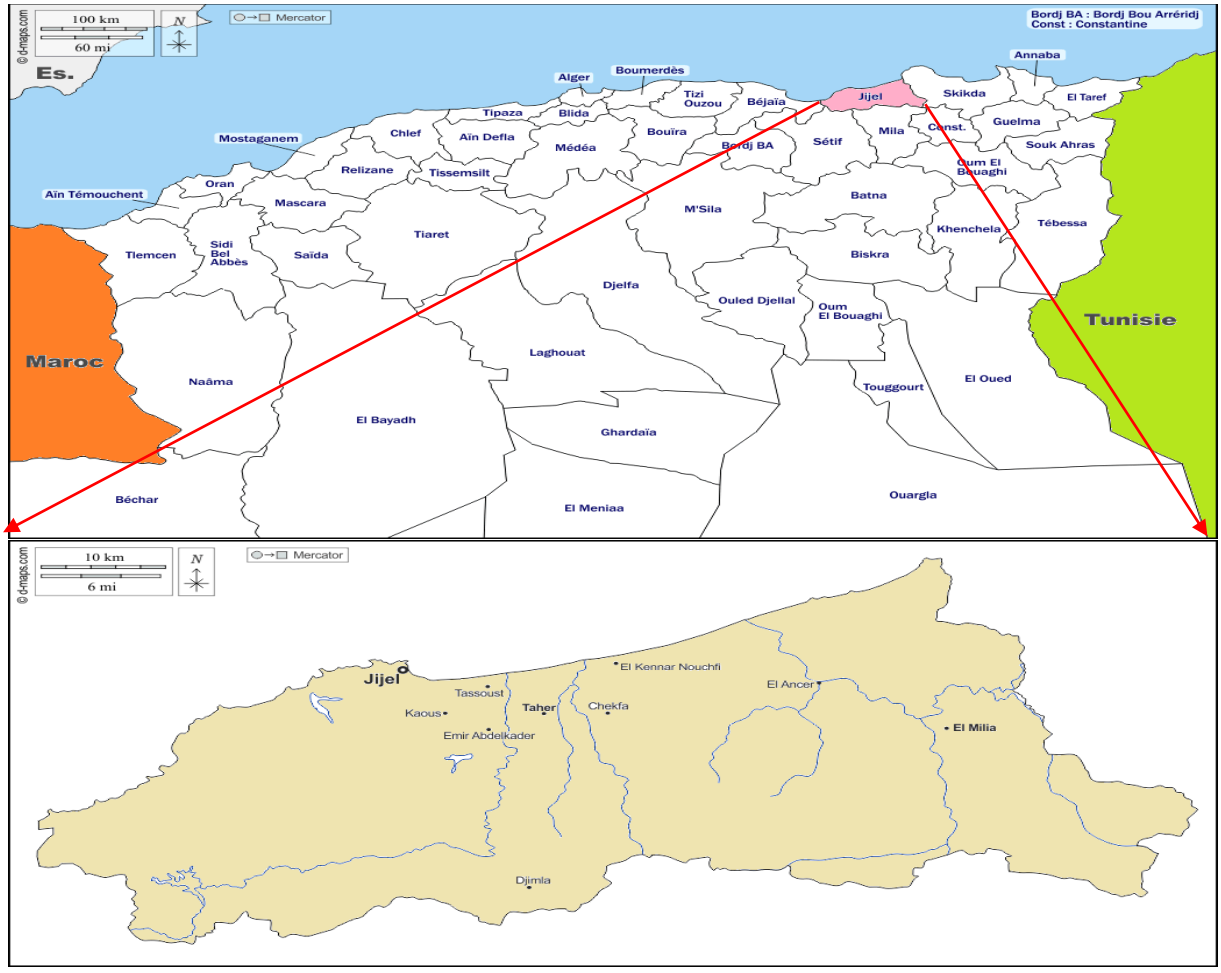

The annual reference evapotranspiration (ET_0) in Jijel Province, calculated using the FAO-56 Penman–Monteith equation over the period 2000–2024, exhibited notable spatial variability across the ten studied stations, reflecting the region's topographic and microclimatic diversity. The highest long-term mean annual ET_0 is observed at El Ancer (1242 mm), followed closely by El Milia (1236 mm) and El Kennar Nouchfi (1225 mm), likely due to their elevated inland positions in the Tell Atlas foothills that experience higher solar radiation exposure and

wind influences. In contrast, lower values were recorded at coastal and lower-elevation sites, such as Emir Abdelkader (1195 mm), Kaous (1198 mm), and Tassoust (1200 mm), where proximity to the Mediterranean Sea and higher humidity moderate the evaporative demand. Intermediate values characterize stations such as Chefka (1218 mm), Jijel (1215 mm), Djimla (1214 mm), and Taher (1207 mm). Across all sites, annual ET_0 ranges from approximately 1093 mm (Djimla, 2018) to 1333 mm (El Ancer, 2022), with an overall provincial average of 1215 mm.

2.2 Data description and preprocessing

Daily meteorological data for 2000–2024 were retrieved from the Open-Meteo Historical Weather API (OPEN-METEO, 2024), which provides access to the datasets. The key input variables were air temperature at 2 m, relative humidity at 2 m, wind speed at 10 m, terrestrial radiation, sunshine duration, and vapor pressure deficit, which were obtained daily for ten representative locations across Jijel regions and subsequently aggregated to daily means or sums as required. For each station, the dataset was chronologically divided into training (70%; 2000–2017), validation (15%; 2018–2021), and testing (15%; 2022–2024) subsets to ensure temporal independence and to facilitate robust model evaluation. All the input features were standardized using the mean and standard deviation computed from the training set. The Pearson correlation matrix of the six meteorological input variables–air temperature at 2 m (°C), relative humidity at 2 m (%), wind speed at 10 m (km/h), sunshine duration (s), terrestrial radiation (W/m²), and vapor pressure deficit (kPa)–are presented in Figure 2.

Figure 2

Pearson correlation heatmap of the six meteorological input variables for ET prediction.

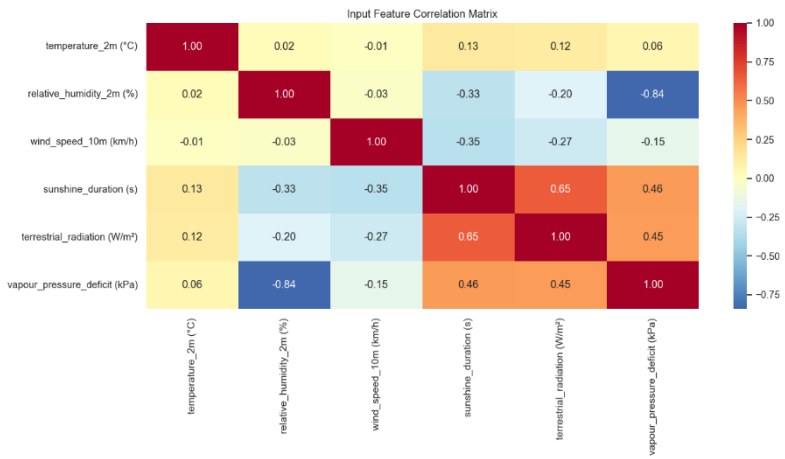

The matrix (Figure 2) reveals several notable relationships between input features. Strong positive correlations were observed between terrestrial radiation and sunshine duration ($r = 0.65$), vapor pressure deficit ($r = 0.45$), and sunshine duration and vapor pressure deficit ($r = 0.46$). These associations are physically consistent because higher solar radiation typically coincides with longer sunshine hours and an increased evaporative demand (higher vapor pressure deficit). Temperature exhibited weak positive correlations with most variables, except for relative humidity, which showed a very weak relationship ($r = 0.02$). The most prominent negative correlation occurred between relative humidity and vapor pressure deficit ($r = -0.84$), reflecting the fundamental inverse relationship between atmospheric moisture content and evaporative demand. Moderate negative correlations were also evident between relative humidity and both sunshine duration ($r = -0.33$) and terrestrial radiation ($r = -0.20$), whereas wind speed displayed weak to moderate negative correlations with several variables, notably sunshine duration ($r = -0.35$).

2.3 Architectures of MLP, RF and GBDT models

2.3.1 Multi-Layer Perceptron (MLP) regressor

The proposed model utilizes the MLPRegressor, a feedforward multilayer perceptron tailored for regression tasks, to predict the FAO reference evapotranspiration (ET_0, in mm) from six normalized meteorological features: temperature at 2 m, relative humidity at 2 m, wind speed at 10 m, sunshine duration, terrestrial radiation, and vapor pressure deficit. The network architecture comprised an input layer (six features), three hidden layers with 128, 64, and 32 neurons (ReLU activation, fully connected), and a single-neuron output layer (linear activation). This tapering design facilitates hierarchical feature extraction, yielding approximately 11,265 trainable parameters. Training employed the Adam optimizer with a mean squared error loss, a maximum of 2000 iterations, early stopping based on validation loss (10% hold-out), and a fixed random state of 42 for reproducibility. The data were divided into 70% training, 15% validation, and 15% testing sets to mitigate overfitting. This straightforward yet effective MLP architecture (Figure 3) leverages gradient-based learning to capture the nonlinear relationships in tabular climate data.

Figure 3

Architecture of Multilayer Perceptron (MLP) regressor for ET_0 prediction.

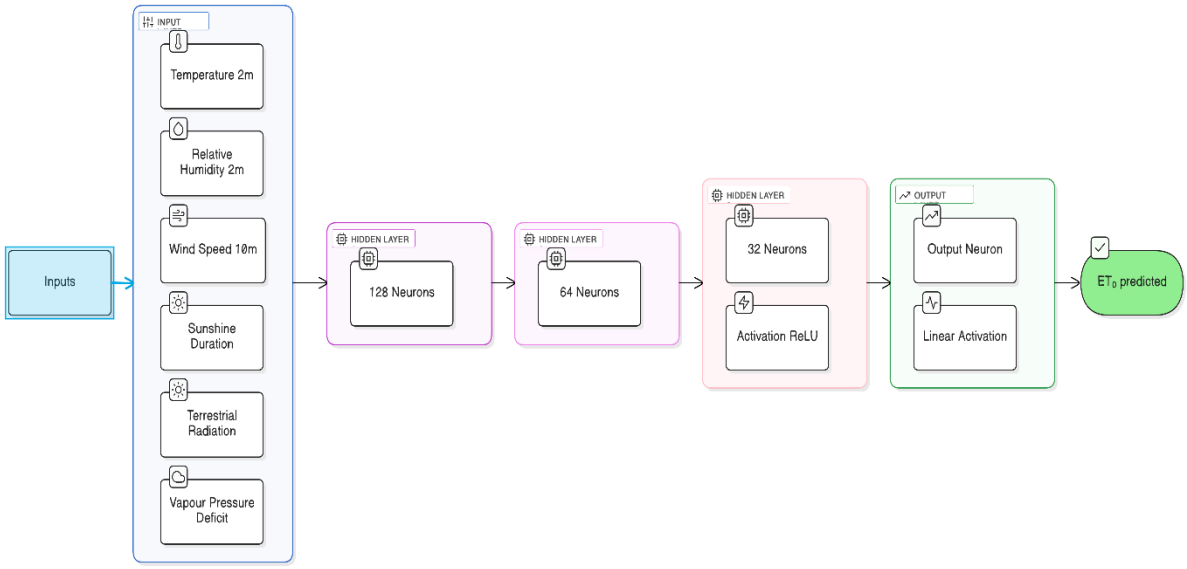

2.3.2 Random forest regressor

The proposed model employs scikit-learn's RandomForestRegressor, an ensemble method that constructs 100 independent decision trees and averages their predictions to yield robust regression outputs with a reduced variance. This approach is well suited for capturing complex, non-linear interactions in environmental datasets, such as the six meteorological features used here to predict the FAO reference evapotranspiration (ET_0, in mm). Each base learner was a binary CART regression tree grown without pruning to minimize the mean squared error at each split, utilizing the full feature set (n_features=6) by default. Diversity is introduced through bootstrap aggregating (bagging), where each tree is trained on a random subset of the data sampled with replacement, combined with inherent randomness in tree construction (Figure 4).

The final prediction was obtained by averaging the outputs across all trees, enhancing the generalization, and mitigating overfitting. A fixed random state of 42 ensures reproducibility, while default hyperparameters maintain simplicity without explicit constraints on tree depth or leaf nodes. This parallel "forest" architecture excels in handling non-linear relationships and feature interactions without requiring feature scaling (though applied here), offering inherent interpretability through individual trees and derivable feature importances, despite the ensemble behaving as a black-box overall.

Figure 4

Architecture of the Random Forest Regressor for ET_0 prediction.

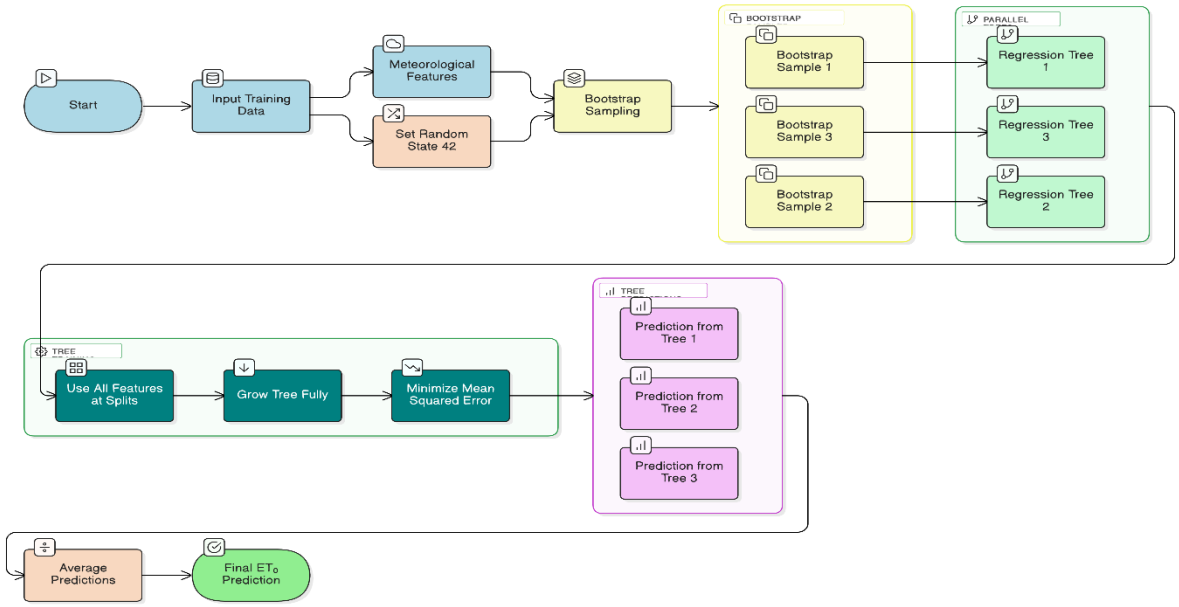

2.3.3 LightGBM regressor

The proposed model employs LightGBM's LGBMRegressor, which is a highly efficient gradient-boosting framework that constructs 100 sequential regression trees using histogram-based splitting for rapid training and enhanced performance on structured datasets. This approach is particularly effective for modeling complex interactions among the six meteorological input features to predict FAO reference evapotranspiration (ET_0, in mm). This architecture utilizes leaf-wise tree growth, enabling deeper and more accurate trees with fewer nodes than level-wise methods. Each tree fit the negative gradients (residuals) of the mean squared error loss, starting from an initial prediction of the target mean, with contributions shrunk by a default learning rate of 0.1. Optimizations include gradient-based one-side sampling (GOSS) and exclusive feature bundling (EFB), although the latter has a limited impact on this dense, low-dimensional (six-feature) dataset. A fixed random state of 42 ensures reproducibility (Figure 5), while default parameters maintain simplicity—no explicit constraints on tree depth, leaf count, or regularization ($\lambda_1=\lambda_2=0$)—with subsampling applied for regularization. The final prediction is the additive sum of all tree outputs (adjusted by the learning rate), and the feature importance is derived from split gains, facilitating the interpretation of key drivers such as temperature or radiation. This sequential additive ensemble excels in accuracy and speed on tabular data through innovations such as feature discretization

into histograms, offers superior scalability, and often outperforms traditional methods such as Random Forest while incorporating built-in overfitting mitigation.

Figure 5

Architecture of the LightGBM Regressor for ET_0 Prediction.

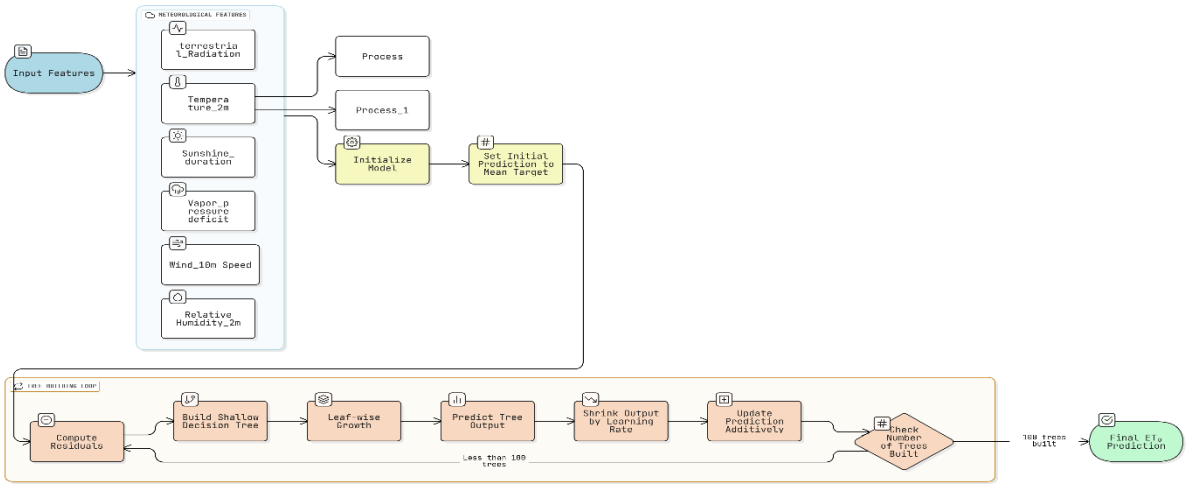

3 RESULTS AND DISCUSSION

3.1 Scatter-plots of MLP, RF, and LightGBM predictions

The scatter plots comparing the predicted and observed daily reference evapotranspiration (ET_0) values demonstrate excellent performance across all three machine learning models: multilayer perceptron (MLP), Random Forest (RF), and Light Gradient Boosting Machine (LightGBM)on the training, validation, and test datasets (Figure 6).

In the training set, all models achieved R^2 values exceeding 0.98, indicating strong agreement between the predictions and observed ET_0 values. Random Forest exhibits the highest training accuracy ($R^2 = 0.997$), with scatter points lying almost perfectly along the 1:1 line across the full range of observed ET_0 (approximately 1–8 mm/day), reflecting minimal bias and very low variance. LightGBM followed closely ($R^2 = 0.990$), while MLP showed slightly greater dispersion ($R^2 = 0.984$), particularly at higher ET_0 values (>6 mm/day). Nevertheless, both models demonstrated robust fitting, with no systematic deviations.

In the validation set, all models maintained a high generalization capability, with R^2 values ranging from 0.980 to 0.983. LightGBM slightly outperformed the others ($R^2 = 0.981$), whereas Random Forest exhibited the smallest decline in training performance. Scatter points

remained tightly clustered around the 1:1 line across the observed ET_0 range (approximately 1–8 mm/day), confirming that the models effectively captured the underlying nonlinear relationships in meteorological input features without substantial overfitting.

The test set provided the most rigorous assessment of generalization to unseen data. All models continued to perform exceptionally well, with R^2 values ≥ 0.978. Notably, MLP achieved the highest test-set performance (R^2 = 0.983), followed closely by LightGBM (R^2 = 0.980), and Random Forest (R^2 = 0.978). Although the Random Forest demonstrates the strongest training fit, its marginally lower performance on the test set suggests a slight degree of overfitting. In contrast, MLP and LightGBM exhibited more consistent behavior across all data partitions, with excellent agreement at both low and high ET_0 values (up to approximately 10 mm/d). Minor deviations in the highest observed values remained within acceptable limits for practical hydrological and agricultural applications.

Figure 6

Scatter plots of MLP, RF, and LightGBM predictions across the training, validation, and test sets

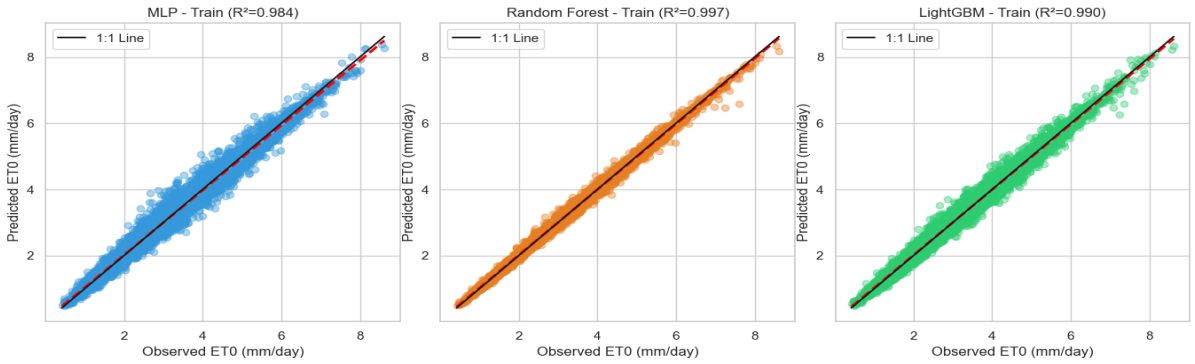

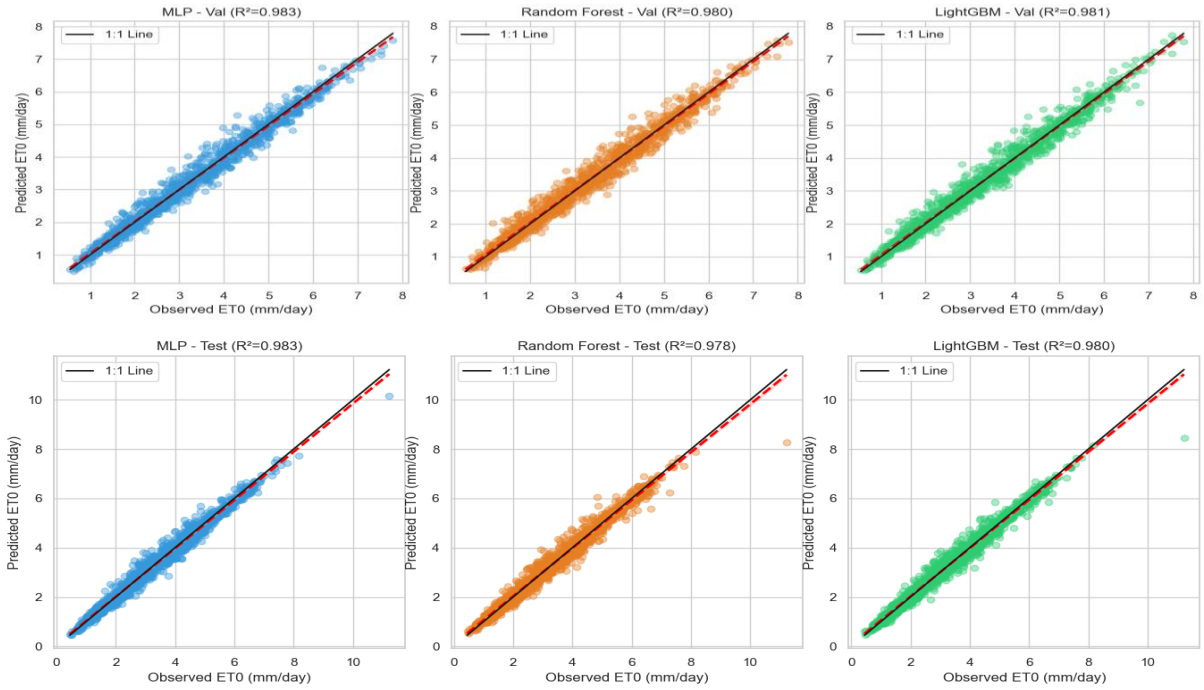

3.2 Residual diagnostics revealing model generalization and potential overfitting in ET_0 prediction

Residual analysis (Figure 7), defined as the difference between predicted and observed daily reference evapotranspiration (ET_0), offers critical insights into model performance beyond aggregate metrics, such as the coefficient of determination (R^2), enabling the identification of systematic biases, heteroscedasticity, and potential overfitting across the training, validation, and test datasets (Figures X–Y). On the training set, residuals for all three models—Multi-Layer Perceptron (MLP), Random Forest (RF), and Light Gradient Boosting Machine (LightGBM)—are symmetrically distributed around zero, indicating unbiased predictions; MLP exhibits homoscedastic behavior with residuals predominantly within ±0.5 mm/day and only isolated outliers exceeding ±0.8 mm/day, while RF shows the tightest clustering (within ±0.3 mm/day) and LightGBM displays slightly greater but still symmetric dispersion (mostly within ±0.5 mm/day). In the validation set, residual behavior remains consistent across models with no pronounced heteroscedasticity or systematic bias; MLP and LightGBM residuals are symmetric and largely confined within ±0.5 mm/day, whereas RF exhibits a marginally wider spread (up to ±0.75 mm/day) and a subtle tendency toward positive residuals at lower ET_0 values (6 mm/day), suggesting mild overfitting. The test set, representing the most rigorous evaluation of generalization to unseen data, reveals that MLP and LightGBM maintain well-behaved, symmetric residuals predominantly within ±0.5 mm/day (with only occasional outliers reaching

±1 mm/day), confirming their excellent robustness, whereas RF displays considerably greater dispersion with several large positive outliers (up to +3 mm/day) and a few negative outliers (down to –1 mm/day), primarily at higher ET_0 values (>6 mm/day), highlighting a degree of overfitting despite its superior training fit. Overall, these diagnostics confirm that while RF excels on training data, MLP and LightGBM provide superior generalization with stable, low-magnitude residuals across all partitions, making them more reliable choices for operational ET_0 estimation in the humid Mediterranean climate of Jijel under varying meteorological conditions. Residual analysis across all the datasets revealed no pronounced heteroscedasticity or systematic bias in any model, with residuals symmetrically distributed around zero, which is desirable for hydrological applications. Random Forest achieved the lowest residual spread on the training set (consistent with $R^2 = 0.997$), yet exhibited the largest outliers on the test set, particularly at high ET_0 values (>6 mm/day), indicating mild overfitting. In contrast, MLP and LightGBM displayed consistently stable and symmetric residuals with minimal outliers and low variance across all partitions, confirming superior generalization. These findings suggest that for operational use in precision agriculture and irrigation scheduling in Jijel's humid Mediterranean climate, MLP and LightGBM offer greater reliability, as occasional large residuals in random forests could lead to overestimation of crop water needs during periods of elevated evaporative demand.

Figure 7

Residuals (Predicted – Observed) versus observed ET_0 for MLP, Random Forest, and LightGBM models across training, validation, and test sets.

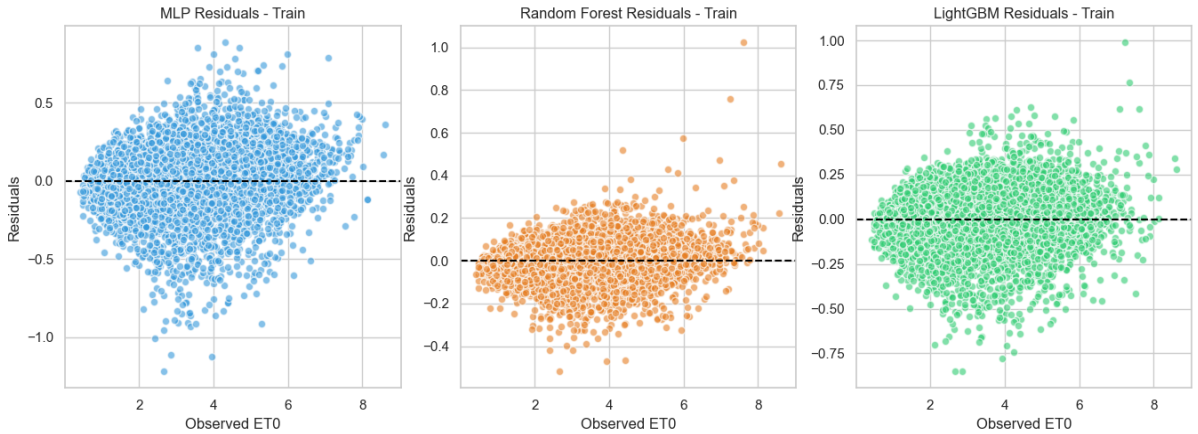

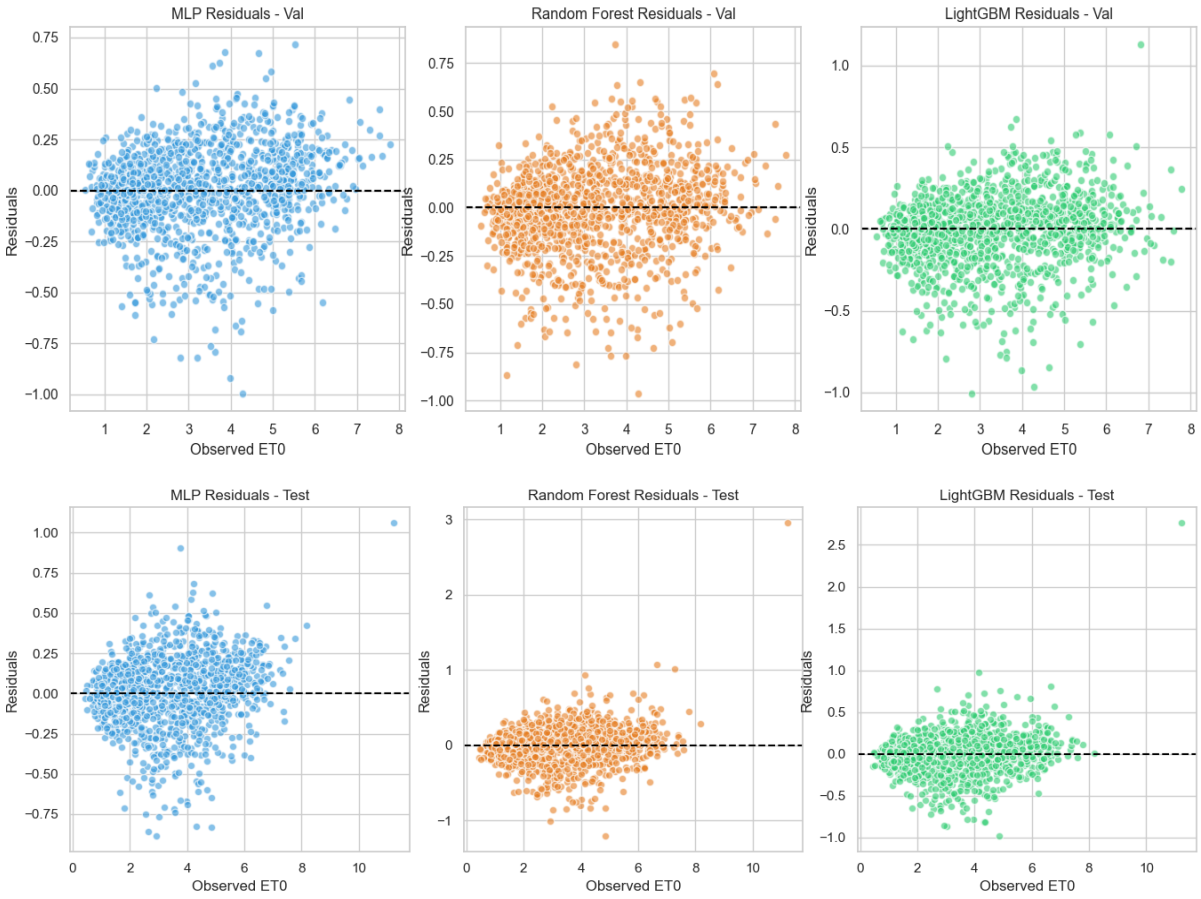

3.3 Performance evaluation of MLP, RF and LGBM models across 10 locations in Jijel

The performance of three machine learning models—Multilayer Perceptron (MLP), Random Forest (RF), and Light Gradient Boosting Machine (LGBM) was comprehensively evaluated for daily FAO-56 reference evapotranspiration (ET_0) estimation across ten representative stations in Jijel Province, Algeria (Jijel – Table 1; Kaous – Table 2; Taher – Table 3; Chekfa – Table 4; Emir Abdelkader – Table 5; Djimla – Table 6; Tassoust – Table 7; El Kennar Nouchfi – Table 8; El Ancer – Table 9; El Milia – Table 10), using standardized metrics: Root Mean Square Error (RMSE), Mean Absolute Error (MAE), Coefficient of Determination (R^2), Nash–Sutcliffe Efficiency (NSE), RMSE-observations Root Sum Ratio (RSR), and Willmott's Index of Agreement (WI) across training, validation, and testing phases (MORIASI et al., 2007, 2015; NASH - SUTCLIFFE, 1970; WILLMOTT et al., 1985). During the training phase, RF consistently exhibited superior performance across all ten stations, achieving the lowest RMSE (ranging from 0.0828 mm/d in Djimla to 0.0869 mm/d in Taher) and MAE, along with the highest R^2 (>0.9986), NSE (>0.9972), and Willmott's index (approaching 0.9995 in Djimla, El Ancer, and El Milia), demonstrating an exceptional fitting

capability. LGBM ranked second with marginally higher errors, whereas MLP showed substantially elevated RMSE and MAE values and lower efficiency coefficients, indicating challenges in capturing nonlinear patterns without overfitting training data. In the validation and testing phases, the model performance converged, yielding robust generalization across regions. On independent test sets (2022–2024), all models performed excellently according to hydrological benchmarks, with $R^2 > 0.988$, NSE > 0.977, RSR < 0.15, and Willmott's index > 0.994 at every station. RF and LGBM generally outperformed MLP, with RF frequently recording the lowest RMSE (e.g., 0.2418 mm/d in Jijel and 0.2159 mm/d in Djimla) and the highest R^2 and NSE, although LGBM occasionally edged ahead in stations such as Chekfa, El Kennar Nouchfi, and El Ancer (lowest test RMSE of 0.2174 mm/d). The strongest overall generalization was observed in Djimla and El Ancer, where NSE exceeded 0.984 and Willmott's index surpassed 0.995, whereas slightly higher errors occurred in Jijel, Taher, and El Kennar Nouchfi, possibly reflecting greater climatic or data heterogeneity.

Overall, Random Forest emerged as the most reliable model across the majority of stations, striking the optimal balance between training accuracy and out-of-sample generalization, closely followed by LGBM. Both tree-based ensemble methods markedly surpassed the MLP architecture, particularly in mitigating overfitting, thereby affirming their superiority for data-driven ET_0 modeling in the diverse humid coastal and foothill environments of Jijel.

Table 1

Evaluation of model performance metrics in the Jijel region

Metric	MLP Train	RF Train	LGBM Train	MLP Val	RF Val	LGBM Val	MLP Test	RF Test	LGBM Test
RMSE	0.2078	0.0863	0.1613	0.2074	0.2207	0.2145	0.2134	0.2418	0.2283
MAE	0.1532	0.0615	0.1195	0.1532	0.1630	0.1572	0.1578	0.1675	0.1599
R^2	0.9918	0.9986	0.9951	0.9913	0.9902	0.9907	0.9914	0.9889	0.9901
NSE	0.9837	0.9972	0.9902	0.9827	0.9804	0.9815	0.9828	0.9779	0.9803
RSR	0.1279	0.0531	0.0992	0.1316	0.1400	0.1361	0.1311	0.1486	0.1403
Willmott	0.9958	0.9993	0.9975	0.9956	0.9950	0.9953	0.9956	0.9944	0.9950

Table 2

Evaluation of model performance metrics in the Kaous region

Metric	MLP Train	RF Train	LGBM Train	MLP Val	RF Val	LGBM Val	MLP Test	RF Test	LGBM Test
RMSE	0.2060	0.0839	0.1579	0.2056	0.2192	0.2118	0.2104	0.2363	0.2248
MAE	0.1512	0.0604	0.1179	0.1526	0.1631	0.1575	0.1549	0.1630	0.1565
R^2	0.9914	0.9986	0.9949	0.9910	0.9897	0.9904	0.9911	0.9888	0.9898
NSE	0.9828	0.9971	0.9899	0.9820	0.9795	0.9809	0.9822	0.9776	0.9797
RSR	0.1311	0.0534	0.1005	0.1342	0.1431	0.1382	0.1333	0.1497	0.1424
Willmott	0.9956	0.9993	0.9974	0.9954	0.9948	0.9951	0.9955	0.9943	0.9948

Table 3

Evaluation of model performance metrics in the Taher region

Metric	MLP Train	RF Train	LGBM Train	MLP Val	RF Val	LGBM Val	MLP Test	RF Test	LGBM Test
RMSE	0.2164	0.0869	0.1611	0.2172	0.2233	0.2148	0.2239	0.2437	0.2327
MAE	0.1628	0.0622	0.1193	0.1653	0.1648	0.1588	0.1698	0.1697	0.1626
R^2	0.9915	0.9986	0.9951	0.9908	0.9900	0.9908	0.9909	0.9888	0.9898
NSE	0.9824	0.9972	0.9903	0.9812	0.9802	0.9816	0.9812	0.9778	0.9797
RSR	0.1326	0.0533	0.0987	0.1371	0.1409	0.1356	0.1370	0.1491	0.1424
Willmott	0.9955	0.9993	0.9975	0.9952	0.9950	0.9953	0.9952	0.9943	0.9948

Table 4

Evaluation of model performance metrics in the Chekfa region

Metric	MLP Train	RF Train	LGBM Train	MLP Val	RF Val	LGBM Val	MLP Test	RF Test	LGBM Test
RMSE	0.2134	0.0858	0.1578	0.2151	0.2218	0.2108	0.2205	0.2408	0.2283
MAE	0.1609	0.0610	0.1173	0.1638	0.1627	0.1549	0.1670	0.1680	0.1608
R^2	0.9921	0.9987	0.9955	0.9914	0.9906	0.9915	0.9915	0.9896	0.9906
NSE	0.9837	0.9974	0.9911	0.9824	0.9813	0.9831	0.9826	0.9793	0.9814
RSR	0.1276	0.0513	0.0943	0.1327	0.1368	0.1300	0.1319	0.1440	0.1366
Willmott	0.9958	0.9993	0.9978	0.9955	0.9952	0.9957	0.9956	0.9947	0.9953

Table 5

Evaluation of model performance metrics in the Emir–Abdulkader region

Metric	MLP Train	RF Train	LGBM Train	MLP Val	RF Val	LGBM Val	MLP Test	RF Test	LGBM Test
RMSE	0.2101	0.0836	0.1569	0.2098	0.2182	0.2103	0.2151	0.2348	0.2220
MAE	0.1561	0.0603	0.1172	0.1583	0.1624	0.1563	0.1606	0.1611	0.1546
R^2	0.9911	0.9986	0.9950	0.9907	0.9898	0.9905	0.9909	0.9889	0.9901
NSE	0.9821	0.9972	0.9900	0.9812	0.9797	0.9811	0.9814	0.9778	0.9802
RSR	0.1339	0.0533	0.1000	0.1371	0.1426	0.1374	0.1364	0.1489	0.1408
Willmott	0.9954	0.9993	0.9975	0.9952	0.9948	0.9952	0.9952	0.9943	0.9949

Table 6

Evaluation of model performance metrics in the Djimla region

Metric	MLP Train	RF Train	LGBM Train	MLP Val	RF Val	LGBM Val	MLP Test	RF Test	LGBM Test
RMSE	0.2115	0.0828	0.1572	0.2144	0.2206	0.2118	0.2064	0.2159	0.2074
MAE	0.1569	0.0604	0.1184	0.1566	0.1620	0.1534	0.1531	0.1576	0.1518
R^2	0.9932	0.9990	0.9962	0.9925	0.9919	0.9926	0.9934	0.9927	0.9932
NSE	0.9863	0.9979	0.9924	0.9848	0.9839	0.9851	0.9866	0.9853	0.9865
RSR	0.1171	0.0458	0.0870	0.1235	0.1270	0.1219	0.1157	0.1211	0.1163
Willmott	0.9965	0.9995	0.9981	0.9961	0.9959	0.9962	0.9966	0.9963	0.9966

Table 7

Evaluation of model performance metrics in the Tassoust region

Metric	MLP Train	RF Train	LGBM Train	MLP Val	RF Val	LGBM Val	MLP Test	RF Test	LGBM Test
RMSE	0.2149	0.0836	0.1572	0.2148	0.2203	0.2102	0.2182	0.2354	0.2246
MAE	0.1594	0.0603	0.1170	0.1614	0.1633	0.1555	0.1631	0.1613	0.1553
R^2	0.9907	0.9986	0.9950	0.9902	0.9897	0.9906	0.9906	0.9889	0.9899
NSE	0.9813	0.9972	0.9900	0.9804	0.9794	0.9812	0.9810	0.9778	0.9798
RSR	0.1366	0.0531	0.0999	0.1401	0.1436	0.1370	0.1380	0.1489	0.1421
Willmott	0.9953	0.9993	0.9975	0.9950	0.9947	0.9952	0.9951	0.9943	0.9948

Table 8

Evaluation of model performance metrics in the El Kennar Nouchfi region

Metric	MLP Train	RF Train	LGBM Train	MLP Val	RF Val	LGBM Val	MLP Test	RF Test	LGBM Test
RMSE	0.2132	0.0857	0.1576	0.2156	0.2225	0.2107	0.2212	0.2423	0.2264
MAE	0.1612	0.0610	0.1172	0.1644	0.1624	0.1554	0.1672	0.1693	0.1608
R^2	0.9923	0.9987	0.9956	0.9915	0.9906	0.9916	0.9916	0.9896	0.9909
NSE	0.9839	0.9974	0.9912	0.9825	0.9813	0.9833	0.9827	0.9792	0.9818
RSR	0.1269	0.0510	0.0938	0.1324	0.1366	0.1294	0.1317	0.1443	0.1348
Willmott	0.9959	0.9993	0.9978	0.9955	0.9953	0.9958	0.9956	0.9947	0.9954

Table 9

Evaluation of model performance metrics in the El Ancer region

Metric	MLP Train	RF Train	LGBM Train	MLP Val	RF Val	LGBM Val	MLP Test	RF Test	LGBM Test
RMSE	0.2213	0.0862	0.1583	0.2231	0.2324	0.2164	0.2255	0.2254	0.2174
MAE	0.1677	0.0619	0.1188	0.1676	0.1688	0.1595	0.1724	0.1654	0.1588
R^2	0.9926	0.9989	0.9961	0.9919	0.9911	0.9923	0.9922	0.9920	0.9925
NSE	0.9848	0.9977	0.9922	0.9836	0.9822	0.9846	0.9840	0.9840	0.9851
RSR	0.1232	0.0480	0.0882	0.1280	0.1333	0.1241	0.1265	0.1265	0.1220
Willmott	0.9961	0.9994	0.9980	0.9958	0.9955	0.9961	0.9959	0.9959	0.9962

Table 10

Evaluation of Model performance metrics in the El Milia region

Metric	MLP Train	RF Train	LGBM Train	MLP Val	RF Val	LGBM Val	MLP Test	RF Test	LGBM Test
RMSE	0.2282	0.0842	0.1550	0.2326	0.2266	0.2097	0.2331	0.2283	0.2186
MAE	0.1690	0.0610	0.1162	0.1695	0.1666	0.1545	0.1750	0.1661	0.1610
R^2	0.9921	0.9989	0.9963	0.9912	0.9917	0.9929	0.9916	0.9919	0.9926
NSE	0.9842	0.9978	0.9927	0.9825	0.9834	0.9858	0.9832	0.9839	0.9852
RSR	0.1259	0.0464	0.0855	0.1322	0.1287	0.1191	0.1297	0.1271	0.1217
Willmott	0.9960	0.9995	0.9982	0.9956	0.9958	0.9964	0.9958	0.9959	0.9963

3.4 Kernel density estimates of residual distributions for MLP, Random Forest, and LightGBM models across training, validation, and test sets

Kernel density estimates (KDE) of the residuals (predicted minus observed FAO-56 ET_0) provide a continuous visualization of error distributions for the multilayer perceptron (MLP), Random Forest (RF), and Light Gradient Boosting Machine (LightGBM) models across training, validation, and independent test datasets (Figure 8), allowing direct assessment of central tendency, dispersion, symmetry, and tail behavior. In the training set, RF produced the narrowest and tallest peak centered at zero (maximum density ≈6), indicative of superior fitting and minimal scatter, followed by LightGBM (peak density ≈3) with a slightly broader yet symmetric distribution, whereas MLP exhibited the widest spread, lower peak, and modestly heavier negative tails, all remaining unbiased and symmetric. In the validation, the three distributions converged markedly, displaying near-identical unimodal, symmetric shapes centered at zero with peak densities of 2.2–2.4 and negligible differences in spread. On the test set, however, MLP and LightGBM yield virtually overlapping, near-Gaussian distributions tightly confined within ±1 mm day^{-1}, whereas RF deviates most from normality with mild positive skewness and an extended positive tail up to +3 mm day^{-1}, revealing occasional substantial overestimations on unseen data. Collectively, although RF achieves the most concentrated residuals during training, this superiority erodes on out-of-sample data, where MLP and LightGBM maintain more stable and near-normal residual structures. This offers advantages for uncertainty quantification and operational reliability in hydrological and agricultural applications, where extreme ET_0 prediction errors can significantly affect irrigation scheduling, crop water requirements, and regional water balance assessments.

Figure 8

Residual Distribution Analysis: Kernel Density Functions for MLP, Random Forest, and LightGBM across Data Partitions.

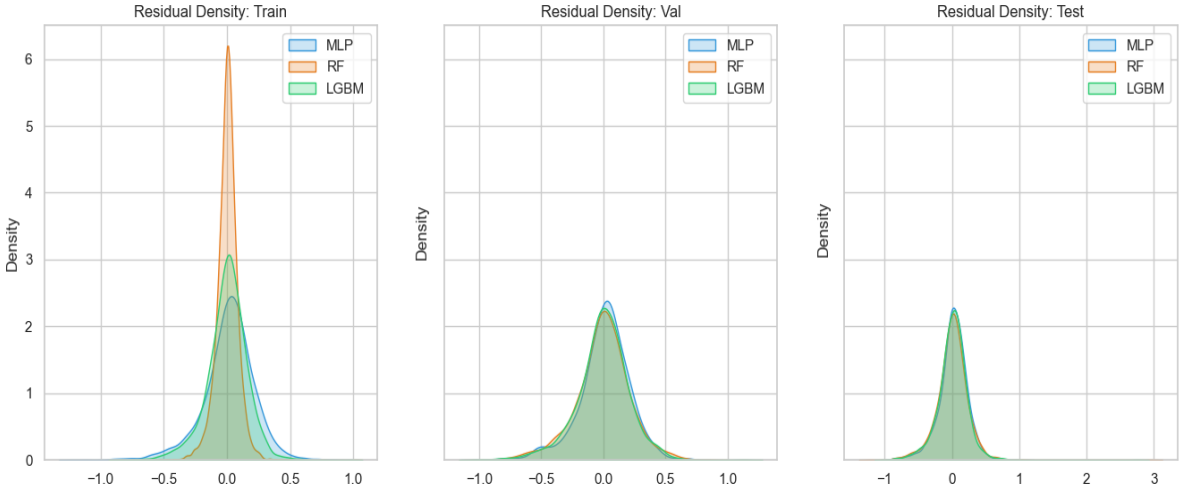

3.5 Time-series comparison of observed and predicted et₀ and residual errors

Time-series plots of the first 50 samples (Figure 9) from each dataset partition (training, validation, and independent test) illustrate the predictive performance of the Multi-Layer Perceptron (MLP; blue dashed line), Random Forest (RF; orange dashed line), and Light Gradient Boosting Machine (LightGBM; green dashed line) models against observed FAO-56 Penman–Monteith ET₀ values (solid black line), with corresponding residual errors (predicted minus observed) displayed as stacked bars below (Figure X). On the training set, all models closely replicate observed ET₀ fluctuations (2–6 mm day^{-1}), with residuals predominantly confined to ±0.3 mm day^{-1} and RF demonstrating the tightest agreement, followed by LightGBM and MLP, consistent with its superior in-sample metrics. In the validation partition, predictions from all three models faithfully capture peak and trough dynamics with residuals generally within ±0.4 mm day^{-1} and no evident bias, though LightGBM and MLP occasionally exhibit marginally smaller errors during rapid transitions. On the unseen test set, MLP and LightGBM sustain excellent temporal tracking with residuals mostly within ±0.3 mm day^{-1}, whereas RF displays larger deviations—particularly during higher ET₀ episodes (reaching ±0.5 mm day^{-1} or more)—indicating mild overfitting. Collectively, these visualizations underscore the strong capability of all models to reproduce cyclic and irregular ET₀ patterns essential for irrigation scheduling. However, while RF excelled on training data, MLP and LightGBM provided more consistent and reliable predictions on independent data, with reduced residual

variability, rendering them particularly suitable for operational reference evapotranspiration estimation in the humid Mediterranean environment of Jijel Province.

Figure 9

Time-series comparison of observed and predicted reference evapotranspiration (ET_0) and corresponding residual errors for MLP, Random Forest, and LightGBM models on training, validation, and test sets (First 50 samples)

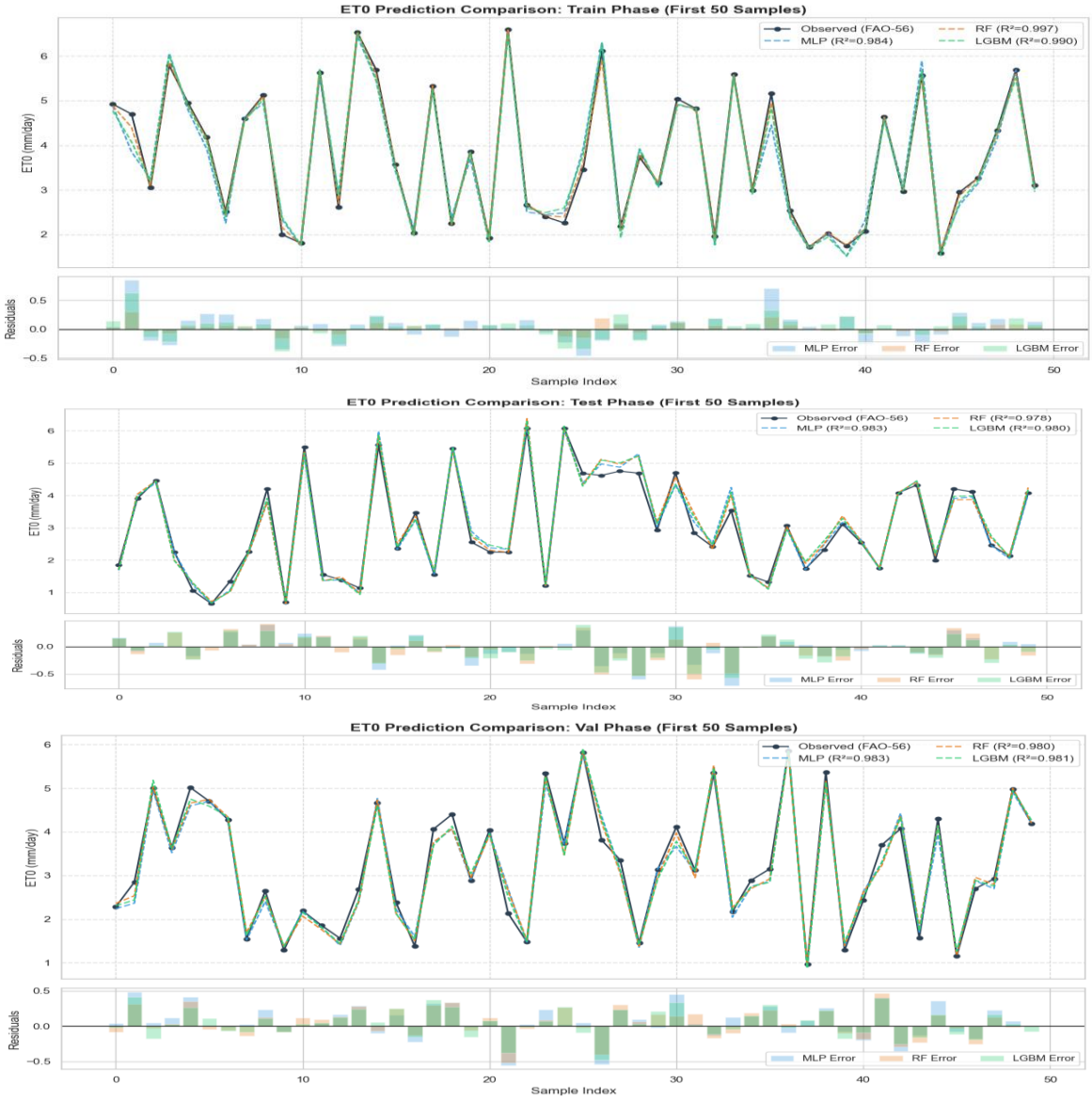

3.6 Temporal trends and variability in annual reference evapotranspiration across Jijel (2000-2024)

Long-term analysis of the annual regional mean reference evapotranspiration (ET_0) for the 2000–2024 period revealed a stable temporal pattern characterized by significant inter-annual variability rather than a sustained monotonic trend. Statistical assessment using the nonparametric Mann–Kendall test yielded a p-value of 0.907 (Figure 10), which substantially exceeded the conventional significance threshold ($\alpha = 0.05$), thereby failing to reject the null hypothesis of no trend. Sen's slope estimator indicated a negligible positive rate of change of 0.083 mm/year, corresponding to a total cumulative increase of only 0.16% over the 25-year study period. Furthermore, the 95% confidence interval for the slope ([-2.736, 2.305]) was zero, reinforcing the conclusion that the observed fluctuations were statistically indistinguishable from the natural climatic noise. This stability suggests that the regional evapotranspiration has remained in a state of relative equilibrium, where the potential impacts of rising temperatures may have been mitigated by opposing trends in other aerodynamic or radiative drivers, a phenomenon consistent with the 'evaporation paradox' observed in various Mediterranean contexts.

Figure 10

Assessment of temporal stability in regional annual ET_0: Integration of descriptive statistics and trend analysis for 2000–2024

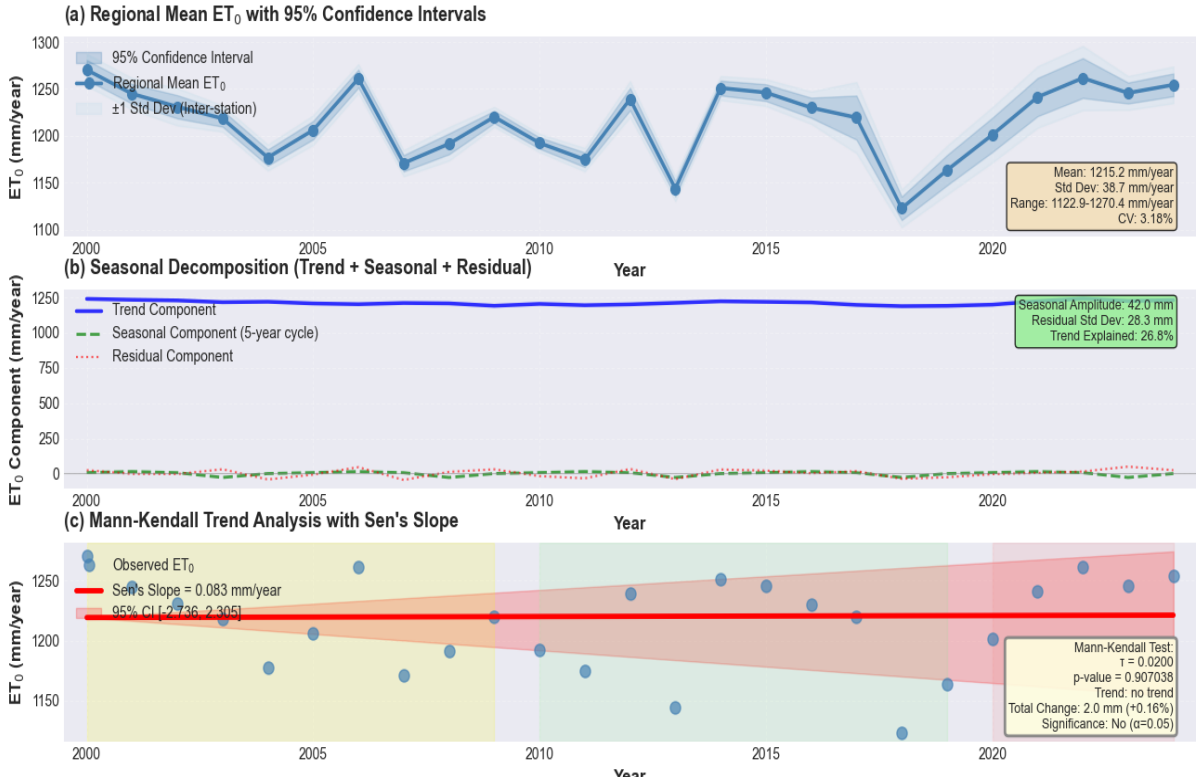

3.7 Spatial and interannual variability of reference evapotranspiration in Jijel region

The spatial and temporal patterns of the mean monthly reference evapotranspiration (ET_0) across Jijel Province revealed substantial heterogeneity driven by topographic and microclimatic influences (Figures 11, 12, and 13). Long-term averages exhibit a clear east–west and elevation-related gradient, with maximum values exceeding 103 mm month^{-1} at inland foothill stations such as El Ancer and El Milia, and lower values near 100 mm month^{-1} along the coastal fringe, reflecting the moderating effect of maritime humidity and cooler temperatures. Over the 25-year period (2000–2024), the region experienced a modest overall decline in mean monthly ET_0 (−1.366 mm month^{-1} regionally), contrasting with increasing trends reported in Algeria's semi-arid interior. Year-to-year differences display considerable interannual variability, with Δ ET_0 frequently ranging between −8 and +9 mm month^{-1} and exhibiting spatially coherent anomalies—most prominently negative shifts in 2006–2007, 2012–2013, and 2017–2018, and positive shifts in 2005–2006, 2011–2012, and 2018–2019—often centered on specific stations (e.g., Djimla and El Ancer). This localized clustering suggests the influence of orographic effects and differential responses to synoptic weather

patterns, underscoring the importance of station-specific modeling approaches for accurate ET₀ estimation in this topographically complex humid coastal region.

Figure 11

Spatial distribution and temporal variability of mean monthly reference evapotranspiration (ET₀) in Jijel region, Algeria (2000–2006).

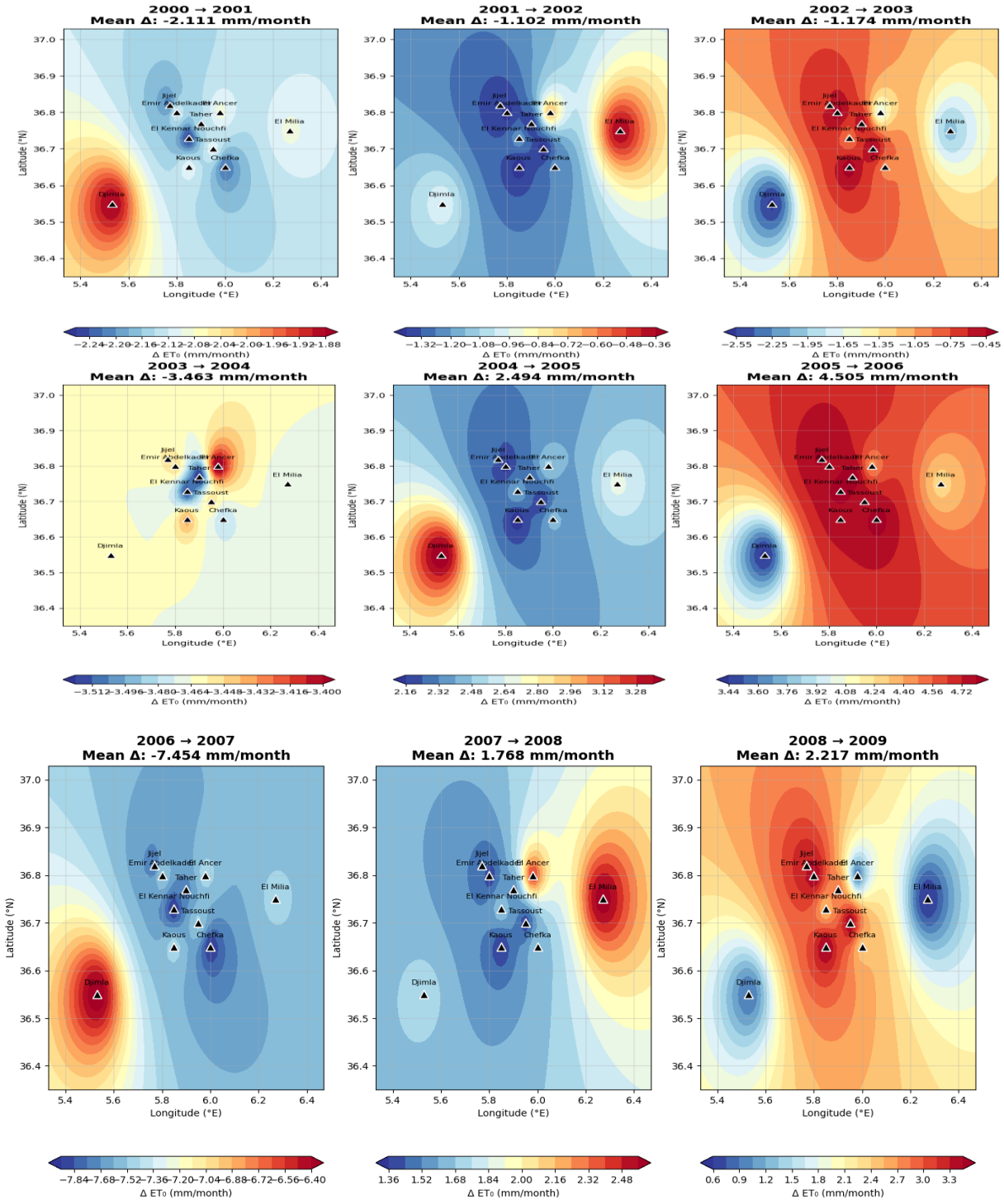

Figure 12

Spatial distribution and temporal variability of mean monthly reference evapotranspiration (ET_0) in Jijel region, Algeria (2006–2015).

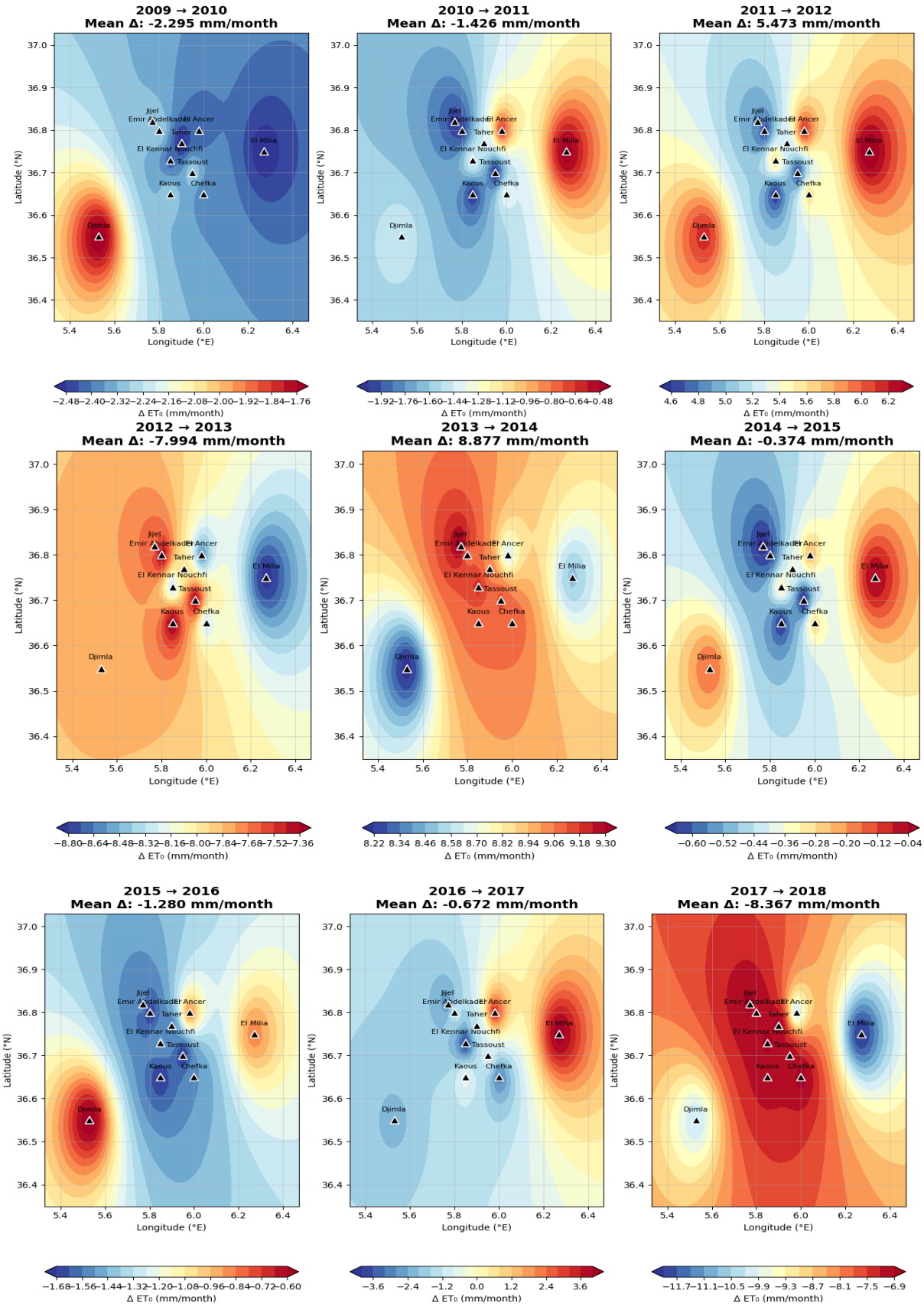

Figure 13

Spatial distribution and temporal variability of mean monthly reference evapotranspiration (ET₀) in Jijel region, Algeria (2015–2024).

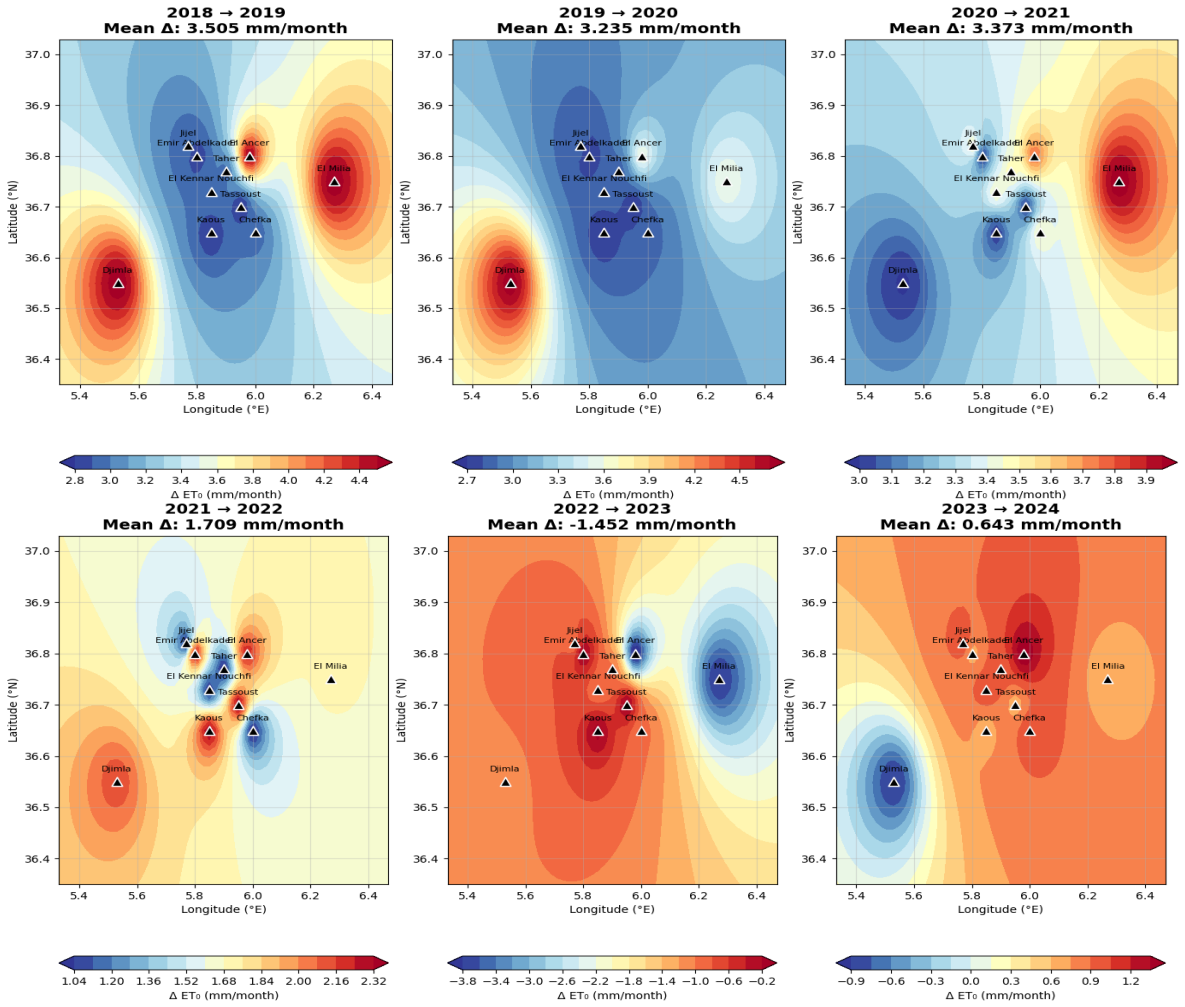

4 CONCLUSION

This study assessed the performance of three machine learning models, multilayer perceptron (MLP), Random Forest (RF), and Light Gradient Boosting Machine (LightGBM), for daily FAO-56 reference evapotranspiration (ET_0) estimation in the humid Mediterranean region of Jijel, northeastern Algeria, using meteorological data from ten stations over the period 2000–2024. All models achieved high predictive accuracy, with coefficients of determination (R^2) exceeding 0.97 across all datasets.

RF showed the strongest training performance ($R^2 = 0.997$, RMSE ≈ 0.09 mm day^{-1}), indicating excellent fitting capability. However, its generalization was slightly weaker on independent test data ($R^2 \approx 0.979$, RMSE up to 0.24 mm day^{-1}), suggesting mild overfitting, particularly during high evaporative demand periods. In contrast, MLP demonstrated the most

stable generalization performance (test $R^2 = 0.983$, RMSE = 0.21 mm day^{-1}, NSE = 0.983), closely followed by LightGBM (test $R^2 \approx 0.980$, RMSE ≈ 0.23 mm day^{-1}). Willmott's index consistently exceeded 0.994 for all models.

Spatial analysis indicated mean annual ET_0 values ranging from approximately 1,195 to 1,242 mm across the Jijel region. Trend analysis using the Mann–Kendall test revealed no significant long-term trend ($p = 0.907$), with a negligible Sen's slope of 0.083 mm $year^{-1}$. Overall, MLP and LightGBM are recommended for reliable operational ET_0 estimation in humid Mediterranean climates.

FUNDING STATEMENT

The author declares that no funds, grants, or other support was received during the preparation of this manuscript.

ETHICAL COMPLIANCE

Not applicable. This study did not involve human participants, human data, animals or tissues.

DATA AVAILABILITY STATEMENT

The meteorological data used in this study were obtained from the Open-Meteo Historical Weather API (Open-Meteo, 2024), which is a publicly available reanalysis dataset accessible at https://open-meteo.com/en/docs/historical-weather-api. The derived data and codes supporting the findings of this study are available from the corresponding author upon reasonable request.

AUTHOR CONTRIBUTIONS

Assia Meziani: Conceptualization, Methodology, Data curation, formal analysis, Investigation, Visualization, Writing – original draft, writing – review, and editing.

DATA AVAILABILITY

All datasets relevant to this study's findings are fully available within the article

REFERENCES

Abdullah, S. S., Malek, M. A., Abdullah, N. S., Kisi, O., & Yap, K. S. (2015). Extreme learning machines: A new approach for prediction of reference evapotranspiration. Journal of Hydrology, 527, 184–195. https://doi.org/10.1016/j.jhydrol.2015.04.073

Acharki, S., Raza, A., Vishwakarma, D. K., ET AL. (2025). Comparative assessment of empirical and hybrid machine learning models for estimating daily reference evapotranspiration in sub-humid and semi-arid climates. Scientific Reports, 15, 2542. https://doi.org/10.1038/s41598-024-83859-6

Achite, M., Jehanzaib, M., Sattari, M. T., Toubal, A. K., Elshaboury, N., Wałęga, A., Krakauer, N., Yoo, J.-Y., & Kim, T.-W. (2022). Modern techniques to modeling reference evapotranspiration in a semiarid area are based on ANN and GEP models. Water, 14(1210). https://doi.org/10.3390/w14081210

Agrawal, Y., Kumar, M., Ananthakrishnan, S., Kumarapuram, G. (2022). Evapotranspiration modeling using different tree based ensembled machine learning algorithm. Water Resources Management, 36(3), 1025–1042. https://doi.org/10.1007/s11269-022-03067-7

Al Hasani, A. A. J. & Shahid, S. (2024). Development of radiation- and temperature-based empirical models for accurate daily reference evapotranspiration estimation in Iraq. Stochastic Environmental Research and Risk Assessment, 38(8), 3127–3148. https://doi.org/10.1007/s00477-024-02736-w

Allen, R. G., Pereira, L. S., Raes, D., Smith, M. (1998). Crop evapotranspiration - Guidelines for computing crop water requirements - FAO Irrigation and drainage paper 56. FAO. https://www.fao.org/4/x0490e/x0490e00.htm

Aly, M. S., Darwish, S. M., & Aly, A. A. (2024). High-performance machine learning approach for reference evapotranspiration estimation. Stochastic Environmental Research and Risk Assessment, 38, 689–713. https://doi.org/10.1007/s00477-023-02594-y

Boukhali, Y., Kabbaj, M. N., Benbrahim, M. (2025). Evapotranspiration estimation using deep learning models for robust sensor performance. Franklin Open, 11, 100335. https://doi.org/10.1016/j.fraope.2025.100335

Bouregaa T. (2025). Trends in climatic variables and machine learning-based reference evapotranspiration predictions in key cereal-producing regions of Algeria. Theoretical and Applied Climatology 156, 351. https://doi.org/10.1007/s00704-025-05561-5

Boutellis, T., Bouchair, A. (2022). Predictive capacity analysis for outdoor thermal comfort assessments: A case study of Jijel City, Algeria. Journal of Advanced Research in Fluid Mechanics and Thermal Sciences 98(1), 18–41. https://doi.org/10.37934/arfmts.98.1.1841

Chang, Y., Zhang, C., Huang, J., Chang, H., Wang, C. (2025). Machine learning for reference crop evapotranspiration modeling: a state-of-the-art review and future directions. Agronomy, 15, 2038. https://doi.org/10.3390/agronomy15092038

Chen, Z., Zhu, Z., Jiang, H., & Sun, S. (2020). Estimating daily reference evapotranspiration based on limited meteorological data using deep learning and classical machine learning

methods. Journal of Hydrology, 591, 125286. https://doi.org/10.1016/j.jhydrol.2020.125286

Di Nunno, F., Granata, F. (2023). Future trends in reference evapotranspiration in Sicily based on CORDEX data and machine learning algorithms. Agricultural Water Management, 280, 108232. https://doi.org/10.1016/j.agwat.2023.108232

D-MAPS.COM. (2024). Free maps of Jijel Province, Algeria (online cartographic resources). https://d-maps.com

Elbeltagi, A., Heddam, S., Katipoğlu, O. M., Alsumaiei, A. A., AL Mukhtar, M. (2024). Advanced long-term actual evapotranspiration estimation in humid climates for 1958–2021 based on machine-learning models enhanced by the RReliefF algorithm. Journal of Hydrology: Regional Studies 56: 102043. https://doi.org/10.1016/j.ejrh.2024.102043

Fan, J., Wu, L., Zhang, F., Cai, H., Ma, X., & Bai, H. (2018). Evaluation of SVM, ELM, and four tree-based ensemble models for predicting daily reference evapotranspiration using limited meteorological data in different climates in China. Agricultural and Forest Meteorology, 252, 225–241. https://doi.org/10.1016/j.agrformet.2018.08.019

Feng, Y., Cui, N., Zhao, L., Hu, X., & Gong, D. (2016). Comparison of ELM, GANN, WNN, and empirical models for estimating reference evapotranspiration in the humid region of Southwest China. Journal of Hydrology, 536, 376–383. https://doi.org/10.1016/j.jhydrol.2016.02.053

Gocić, M., Motamedi, S., Shamshirband, S., Petković, D., CH, S., Hashim, R., & ARIF, M. (2015). Soft computing approaches for forecasting reference evapotranspiration. Computers and Electronics in Agriculture, 113, 164–173. https://doi.org/10.1016/j.compag.2015.02.010

Hargreaves, G. H. and Samani, Z. A. (1985). Reference crop evapotranspiration from temperature. Applied Engineering in Agriculture, 1, 96–99. https://doi.org/10.13031/2013.26773

Heramb, P., Ramana RAO, K. V., Subeesh, A., Srivastava, A. (2023). Predictive modelling of reference evapotranspiration using machine learning models coupled with Grey Wolf Optimizer. Water, 15(5), 856. https://doi.org/10.3390/w15050856

Karimi, S., Shiri, J., & Marti, P. (2020). Supplanting missing climatic inputs in classical and random forest models for estimating reference evapotranspiration in humid coastal areas of Iran. Computers and Electronics in Agriculture 178, 105633. https://doi.org/10.1016/j.compag.2020.105633

Kartal, V. (2024). Prediction of monthly evapotranspiration by artificial neural network model development using the Levenberg–Marquardt method in Elazig, Turkey. Environmental Science and Pollution Research, 31(14), 20953–20969. https://doi.org/10.1007/s11356-024-32464-1

Kerdoud, A. (2017). Vulnerabilité à la pollution des eaux de la plaine alluviale d'oued Nil Wilaya de Jijel (N.E. Algérien) [Master's thesis, Université Mohamed Seddik Ben Yahia, Jijel]. http://dspace.univ-jijel.dz:8080/xmlui/bitstream/handle/123456789/2091/M-Eau.Env.%2010-17.pdf?sequence=1

Kisi, O., & Alizamir, M. (2018). Modelling reference evapotranspiration using a new wavelet conjunction heuristic method: wavelet extreme learning machine vs. wavelet neural networks. Agricultural and Forest Meteorology, 263, 41–48. https://doi.org/10.1016/j.agrformet.2018.08.007

Ladlani, I., Houichi, L., Djemili, L., Heddam, S., & Belouz, K. (2012). Modeling daily reference evapotranspiration (ET_0) in the north of Algeria using generalized regression neural networks (GRNN) and radial basis function neural networks (RBFNN): A comparative study. Meteorology and Atmospheric Physics 118(3–4), 163–178. https://doi.org/10.1007/s00703-012-0205-9

Liang, Y., Feng, D., & Sun, Z. (2023). Comparison of four machine learning models for forecasting daily reference evaporation based on public weather forecast data [preprint]. Discussion of Hydrology and Earth System Sciences https://doi.org/10.5194/hess-2023-158

Malik, A., Saggi, M. K., Rehman, S., Sajjad, H., Inyurt, S., Bhatia, A. S., Rajarajeswari, P., Farooque, A. A., Oudah, A. Y., Yaseen, Z. M., Hoat, D. M. (2022). Deep learning versus gradient boosting machine for pan evaporation prediction. Engineering Applications of Computational Fluid Mechanics, 16(1), 570–587. https://doi.org/10.1080/19942060.2022.2027273

Mandal, N., Chanda, K. (2023). Performance of machine learning algorithms for multi-step-ahead prediction of reference evapotranspiration across various agro-climatic zones and cropping seasons. Journal of Hydrology, 620 (Part A), 129418. https://doi.org/10.1016/j.jhydrol.2023.129418

Mehdizadeh, S. (2018). Estimation of daily reference evapotranspiration (ET_0) using artificial intelligence methods: Offering a new approach for lagged ET_0 data-based modeling. Journal of Hydrology, 559, 794–812. https://doi.org/10.1016/j.jhydrol.2018.02.060

Merniz, N., Tahar, A., Benmehaia, A. M. (2019). Statistical assessment of rainfall variability and trends in northeastern Algeria. Journal of Water and Land Development 40(I–III): 87–96. https://doi.org/10.2478/jwld-2019-0009

Mokhtari, H., Benzaouia, M., Hajji, B., Ayadi, N., & Chaabane, K. (2025). Machine learning forecasting approaches for evapotranspiration: a comparative analysis. In B. Hajji, A. Gagliano, A. Mellit, A. Rabhi, and M. Calì (eds.) Proceedings of the 4th International Conference on Electronic Engineering and Renewable Energy Systems—Volume 1 (ICEERE 2024) (pp. 465–475). Springer. https://doi.org/10.1007/978-981-96-0644-3_42

Monteith, J. L. (1965). Evaporation and environment. Symposia of the Society for Experimental Biology, 19, 205–234. https://repository.rothamsted.ac.uk/item/8v5v7/evaporation-and-environment

Moriasi, D.N., Arnold, J.G., Van Liew, M.W., Bingner, R.L., Harmel, R.D., Veith, T.L. (2007). Model evaluation guidelines for systematic quantification of accuracy in watershed simulations. Transactions of the ASABE, 50(3), 885–900. https://doi.org/10.13031/2013.23153

Moriasi, D.N., Gitau, M.W., Pai, N., Daggupati, P. (2015). Hydrologic and water quality models: Performance measures and evaluation criteria. Transactions of the ASABE, 58(6), 1763–1785. https://doi.org/10.13031/trans.58.10715

Nash, J. E., and Sutcliffe, J. (1970). River flow forecasting through conceptual models Part I — A discussion of principles. Journal of Hydrology 10(3): 282–290. https://doi.org/10.1016/0022-1694(70)90255-6

Open-Meteo. (2024). Open-Meteo.com. Historical Weather API [Dataset]. https://open-meteo.com/en/docs/historical-weather-api

Patel, A., Ali, S. T., and Pandey, M. K. (2025). Estimation of reference evapotranspiration using ensemble machine-learning models based on regional scenarios. Applied Water Science, 15, 307. https://doi.org/10.1007/s13201-025-02654-4

Penman, H. L. (1948). Natural evaporation from open water, bare soil, and grass. Proceedings of the Royal Society of London. Series A, Mathematical and Physical Sciences 193(1032), 120–145. https://doi.org/10.1098/rspa.1948.0037

Rodrigues, G. C., Braga, R. P. (2021). A simple procedure to estimate reference evapotranspiration during the irrigation season in a hot summer Mediterranean climate. Sustainability 13(1), 349. https://doi.org/10.3390/su13010349

Shiri, J. (2017). Evaluation of FAO56 PM, empirical, semi-empirical, and gene expression programming approaches for estimating daily reference evapotranspiration in hyper-arid regions of Iran. Agricultural Water Management, 188, 101–114. https://doi.org/10.1016/j.agwat.2017.04.009

Stefanidis, S., Ioannou, K., Proutsos, N., Karmiris, I., Stefanidis, P. (2025). Comparative analysis of machine learning algorithms for potential evapotranspiration estimation using limited data from a high-altitude Mediterranean forest. Atmosphere 16(7), 851. https://doi.org/10.3390/atmos16070851

Szczepanek, R. (2022). Daily streamflow forecasting in mountainous catchments using XGBoost, LightGBM, and CatBoost. Hydrology 9(12): 226. https://doi.org/10.3390/hydrology9120226

Tikhamarine, Y., Malik, A., Kumar, A., Souag Gamane, D., Kisi, O. (2020). Estimation of monthly reference evapotranspiration using novel hybrid machine learning approaches. Hydrological Sciences Journal 64(15): 1824–1842. https://doi.org/10.1080/02626667.2019.1678750

Troncoso García, A. R., Brito, I. S., Troncoso, A., & Martínez Álvarez, F. (2023). Explainable hybrid deep learning and Coronavirus Optimization Algorithm for improving evapotranspiration forecasting. Computers and Electronics in Agriculture, 215, 108387. https://doi.org/10.1016/j.compag.2023.108387

Valiantzas, J. D. (2013). Simplified forms for the standardized FAO 56 Penman–Monteith reference evapotranspiration using limited weather data. Journal of Hydrology, 505, 13–23. https://doi.org/10.1016/j.jhydrol.2013.09.005

Willmott, C.J., Rowe, C.M., Mintz, Y. (1985). Climatology of the terrestrial seasonal water cycle. Journal of Climatology, 5(6), 589–606. https://doi.org/10.1002/joc.3370050602

Wu, L., Huang, G., Fan, J., Ma, X., Zhou, H., & Zeng, W. (2020). Hybrid extreme learning machine with metaheuristic algorithms for monthly pan evaporation prediction. Computers and Electronics in Agriculture, 168, 105115. https://doi.org/10.1016/j.compag.2019.105115

Yao, Z., Wang, Z., Xu, N., Wu, J., & Cui, X. (2025). Interpretable multi-step-ahead prediction of reference evapotranspiration using the attention-based ensemble learning method. Journal of Hydrology, 663, 134084. https://doi.org/10.1016/j.jhydrol.2025.134084

Zhao, X.; Li, Y.; Zhao, Z.; Xing, X.; Feng, G.; Bai, J.; Wang, Y.; Qiu, Z.; Zhang, J. Prediction model for daily reference crop evapotranspiration based on hybrid algorithm in semi-arid regions of China. *Atmosphere*, v. 13, n. 6, p. 922, 2022. DOI : https://doi.org/10.3390/atmos13060922

Zhou, H., Ma, L., Xiang, Y., SU, Y., Li, J., Chen, J., Lu, S., Chen, C., & Wu, Q. (2025). Estimation of reference evapotranspiration using hybrid models optimized by bio-inspired algorithms combined with key meteorological factors. Computers and Electronics in Agriculture, 230, 109862. https://doi.org/10.1016/j.compag.2024.109862

Zhou, Z., Zhao, L., Lin, A., Qin, W., Lu, Y., Li, J., Zhong, Y., & He, L. (2020). Exploring the potential of deep factorization machines and various gradient boosting models for modeling daily reference evapotranspiration in China. Arabian Journal of Geosciences 13: 1287. https://doi.org/10.1007/s12517-020-06293-8

Authors' Contribution

All authors contributed equally to the development of this article.

Data availability

All datasets relevant to this study's findings are fully available within the article.

How to cite this article (APA)

Meziani, A. (2026). MACHINE LEARNING MODELS (MLP, RANDOM FOREST, LIGHTGBM) FOR DAILY ET₀ ESTIMATION WITH LIMITED DATA IN HUMID MEDITERRANEAN REGION (JIJEL) ALGERIA. *Veredas Do Direito*, 23(3), e234267. https://doi.org/10.18623/rvd.v23.n3.4267